Viscous computational fluid dynamics as a relevant decision-making tool for mast-sail aerodynamics

Vincent Chapin, Stéphane Jamme, Patrick Chassaing

Marine Technology, Vol. 42, No. 1, January 2005, pp. 1–10

Marine
Technology

Viscous Computational Fluid Dynamics as a Relevant Decision-Making Tool for Mast-Sail Aerodynamics

V. G. Chapin,[1] **S. Jamme,**[1] and **P. Chassaing**[2]

Viscous computational fluid dynamics based on Reynolds averaged Navier-Stokes (RANS) equations have been used to simulate flow around typical mast-sail geometries. It is shown how these advanced numerical methods are relevant to investigate the complexity of such strongly separated flows. Detailed numerical results have been obtained and compared to experimental ones. Comparative analysis has shown that RANS methods are able to capture the main flow features, such as mast-flow separation, recirculation bubble, bubble reattachment through a laminar-turbulent transition process, and trailing-edge separation. A second part has been devoted to the comparative behavior of these flow features through parameters variations to evaluate the qualitative and quantitative capabilities of RANS methods in mast-sail design optimization. The last part illustrates through two examples how RANS methods may be used to optimize the design of mast-sail geometries and evaluate their relative performances.

Introduction

IMPROVEMENT OF THE AERODYNAMICS of sailing rigs is becoming a crucial challenge for more and more racing yachts (IACC, ocean racing monohull and multihull). Mainsails and jibs are thin, highly cambered sections that are used to generate forces (lift and drag), but there is also a mast in front of the mainsail that greatly affects the aerodynamic performance of the system. This mast at the leading edge of the mainsail radically changes the flow structure on the mainsail, but also on the jib if present, leading to a highly complex flow with separation and recirculation bubble, whatever is the aerodynamic angle of attack. From the fluid-dynamic point of view, it is a three-dimensional, unsteady, separated flow with laminar, transitional, and turbulent regions. From the sailor's point of view, this means that for three-dimensional rig geometries, the total parasitic drag (mast + sails) is of the same order of magnitude as the induced drag of that sail and cannot be neglected. Moreover, sails are made of soft materials, and aeroelastic coupling may take place depending on sailing conditions.

Sail performance depends on a large number of parameters, such as aerodynamic angle of attack ($i = \beta_a + \beta_h - \delta$, with δ the trim angle and β_a the apparent wind angle, β_h the leeway angle), sail shape, sail camber ratio, and position, but also mast shape, orientation, diameter, and so forth. In order to improve sail design for real conditions, performance must be evaluated with sufficient accuracy, taking into account these parameters and real flying shape, before being integrated into aerodynamic models for a velocity prediction program (VPP). Until a few years ago, sail design was done experimentally through trial-and-error practice, full-scale force measurements, and wind-tunnel testing of scale models. Numerical methods were also used but mainly inviscid vortex lattice methods (Milgram 1998).

The America's Cup needs for high-end performances allowed the development of an ambitious program dedicated to the measurement of aerodynamic forces and moments on full-scale IACC in actual sailing conditions. However, following Milgram (1993), it is a long, high-cost, nonconclusive program, as it appears that measurements are not sufficient to generate a mathematical model of sufficient accuracy because of data scatter and uncertainty in the measurement of the wind angle.

Wind-tunnel results on scale models are useful, but the real flying shape of sails is difficult to achieve because of the soft material from which they are made, the difficult problem of rig structural similitude, and the absence of wind-gradient effects in most wind tunnels. Moreover, it is rarely possible to acquire sufficient local measurements, such as wall pressure and skin friction along the sail, to increase our understanding of these complex flows and contribute to the validation of advanced numerical methods.

Besides experimental approaches, numerical methods gives us all flow quantities at all points around sails and should be very useful tools for improving mast-sail design. Unfortunately, inviscid methods, such as the vortex-lattice method, are limited to preliminary design and are not relevant for predicting viscous separated flow with strong adverse pressure gradient as needed to predict mast-sail aerodynamic performances in all sailing conditions. In 2001, Jones and Korpus showed, through an example, the possible deficiency of panel methods compared to RANS methods to predict rig performance variations with sail camber.

Today, advanced numerical predictions of aerodynamic flows around racing yachts based on Reynolds averaged Navier-Stokes (RANS) solvers are accessible with reasonable CPU time because of the continuous increase in computer power of low-cost personal computers. The goal of this paper is to evaluate these viscous RANS methods to predict mast-sail aerodynamic performances and to increase our understanding of these complex flows through detailed flowfields analysis. As we shall see, careful validations have to be done with detailed experimental results to discriminate between relevant and spurious information. Because few published

[1] Fluid Mechanics Department, Ensica, Toulouse, France.
[2] Institut de Mécanique des Fluides de Toulouse, France.
Manuscript received at SNAME headquarters May 2004.

experimental results exist in the literature, this investigation of RANS methods will be restricted to two-dimensional geometries.

We shall provide detailed flow analysis around mast-sail configurations with variable camber ratio and mast diameter for varying aerodynamic angle of attack. RANS simulations will be compared with various wind-tunnel-test databases. Some of them involve lift and drag coefficients measurements alone. The most useful one provides a unique detailed flowfield analysis around a series of typical mast-sail geometries in the large wind tunnel of Southampton University (Wilkinson 1984). A second part will be devoted to a validation of the qualitative behavior of the main flow features as predicted by RANS methods in response to variations of the design parameters. We shall also compare sail performance variations to parameter variations between experimental and numerical results to validate the usefulness of RANS-based methods to do mast-sail design. The last part will emphasize through examples how RANS methods may be used to perform mast-sail analysis and design optimization.

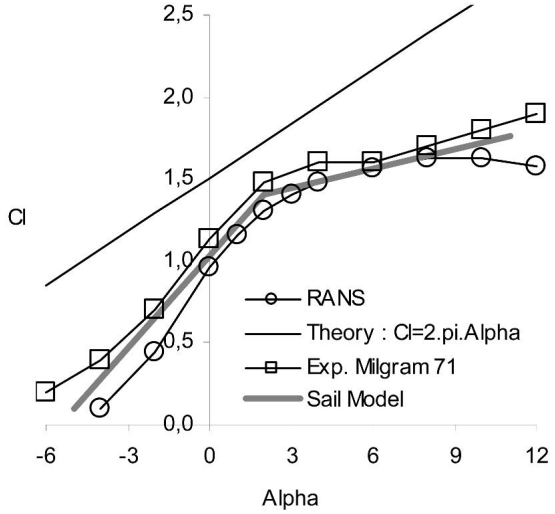

Fig. 1 Lift curve versus incidence angle for thin, high-camber sail section without mast (f/c = 12%)

Sail flow physics: current state of the art

Publications about systematic analysis of two-dimensional sail flows began with Milgram's paper in 1971. In his paper, Milgram considered water-tunnel test results at three Reynolds numbers (6, 9, 12, × 10^5) about thin, highly cambered, rigid sail sections of low aspect ratio (AR = 2.2) without mast. Performances were evaluated through forces and moments measurements with a one-sided dynamometer. Three sail shapes and camber ratio f/c (defined as the ratio of maximum camber f to chord c) ranging from 12% to 18% were tested. The main result of this paper was to show how different are the aerodynamic characteristics of thin highly cambered sections compared to more common, widely studied, moderate-thickness and low-cambered airfoil sections. The lift of thin, highly cambered sections at nearly ideal incidence angle is significantly less than that predicted by thin airfoil theory because of the high camber that generates flow separation. The lift slope is significantly greater than 2π radians for incidence angles lower than the ideal and lower than 2π radians for higher incidence angles. These two main properties of thin, highly cambered sections are presented in Fig. 1.

In 1976, Marchaj provided a critical review of methods for establishing sail coefficients and their practical implications in sailing and yacht performance prediction. In his paper, Marchaj showed how unreliable inviscid vortex lattice methods may be as used by Milgram (1971) to derive analytical

Nomenclature

alpha = aerodynamic angle of attack or incidence angle (also named i)
AR = sail aspect ratio (b^2/S)
b = sail spanwise length
β_a = apparent wind angle
β_h = leeway angle
$\beta_a + \beta_h$ = wind/water angle in the boat reference frame
c = sail chord
C_d, C_l = drag and lift force coefficients
C_r = propulsive force coefficient
C_h = heeling force coefficient
C_p = pressure coefficient
$Cp_{\text{upper\_bubble}}$ = upper surface pressure coefficient in the bubble
δ = trim angle
d = mast diameter
d/c = nondimensional mast diameter or mast diameter ratio
ε_a = aerodynamic drag angle
ε_h = hydrodynamic drag angle
f = sail camber
f/c = sail camber ratio
f_a = aerodynamic lift-to-drag ratio
f_h = hydrodynamic lift-to-drag ratio
F_{da}, F_{la} = aerodynamic drag and lift
F_{ha} = aerodynamic heeling force
F_{ra} = aerodynamic propulsive force
F_{ta} = total aerodynamic force
F_{lh} = hydrodynamic side force
F_{dh} = hydrodynamic resistance
F_{th} = total hydrodynamic force
i = aerodynamic angle of attack or incidence angle (also named alpha)
$L_{\text{lower\_bubble}}$ = lower-surface bubble length
$L_{\text{upper\_bubble}}$ = upper-surface bubble length
$L_{\text{sep\_bdf}}$ = upper-surface trailing-edge separation length
S = sail surface
θ_{stag} = angular position of the stagnation point
θ_{se1} = angular position of the upper surface separation point on the mast
θ_{si1} = angular position of the pressure side separation point on the mast
x_{re1} = location of the suction side reattachment point on the sail
x_{ri1} = location of the pressure side reattachment point on the sail
x_{se2} = location of the suction side separation point on the sail
$//_a$ = axis parallel to the apparent wind
$\perp_a$ = axis orthogonal to the apparent wind
$//_h$ = axis parallel to the boat speed
$\perp_h$ = axis orthogonal to the boat speed

sail coefficients and investigate rig performance. The reason invoked was that they do not take into account mast-sail interference in the pressure and friction drag estimation of the mast-sail drag. Milgram reported that the higher the sail aspect ratio AR is, the higher the yacht speed will be, whereas Marchaj showed through wind-tunnel tests on a simple cat-rig that this may be wrong. This wind-tunnel counterexample emphasizes that the nondimensional mast-diameter d/c may be of greater importance than sail aspect ratio AR in mast-sail performances.

In 1978, in response to Marchaj critics, Milgram tested mast-sail configurations with one mean line (Naca $a = 0.8$), two values of the sail camber ratio ($f/c = 12\%$ and 15%), and four circular masts of different diameters ($d/c = 0\%$, 7%, 15%, 31%) in the same water tunnel as in his previous experiment (Milgram 1971). The sail aspect ratio was always 2.2, and the Reynolds number ranged between 5×10^5 and 14×10^5. It was found that for a given mast ($d/c = 15\%$), the lower camber sail ($f/c = 12\%$) has less drag for a given lift coefficient than the high camber sail ($f/c = 15\%$). Without mast, this was not always the case. For low lift values, the less cambered sail ($f/c = 12\%$) had lower drag, but for high lift values, it had higher drag than the more cambered sail ($f/c = 15\%$). The main conclusion of this experimental study was that "the drag, due to the addition of a mast to the sail, is the result of a complicated flow interaction and is not the sum of mast drag and sail drag as measured separately from each structure in a free stream. For a given mast-sail configuration, the drag coefficient appears as highly correlated with the lift coefficient, and only slightly affected by the combination of wind angle and sail angle required to achieve this lift coefficient." Finally, Milgram concluded that the addition of a mast to a sail raises the friction and pressure drag to the same order of magnitude as the induced drag of that three-dimensional sail.

To summarize, it appears from these papers that it is not reliable to evaluate mast-sail drag with accuracy without taking into account the strong mast-sail interference. From a numerical point of view, viscous nonlinear RANS methods are a good candidate because the mast effect on mast-sail drag is not simply to add a viscous drag component independent to the lift coefficient as is actually hypothesised in most VPPs (Oossanen 1993). The main parameter that governs this strong nonlinear mast-sail interaction is the nondimensional mast diameter d/c.

Some years later in 1984, Wilkinson ran an ambitious experimental program to investigate the mast-sail two-dimensional aerodynamic in a number of typical geometries. To do that, a variable camber instrumented sail model was designed and built to be tested in a 2.13×1.52 m wind tunnel at Southampton University. Data were obtained in the form of static pressure distributions on mast and sail, and velocity profiles in the sail upper-surface boundary layer to investigate flow regimes and structures.

Caponnetto and Castelli in 1998 were probably among the first to use RANS methods to investigate mast-sail flows. Jones and Korpus in 2001 showed that RANS methods, by taking into account viscous effects, may give opposite results to inviscid methods about optimal mainsail camber of an IACC mainsail-jib configuration. Citing Caponnetto and Castelli (1998) and Wynne (2002), Cowles et al in 2003 reported that numerical simulations of upwind sail shapes using RANS-based codes have been shown to be able to predict the level and extent of the separated region aft of the mast, but no additional details were given in the paper. A look at Caponnetto and Castelli's paper (1998) shows that, on a pressure distribution comparison between a Wilkinson experiment and RANS calculations, the suction-side bubble pressure level was well predicted but the bubble length was underestimated.

In this paper, we have investigated how RANS-based codes will enable better sail and mast designs for highly competitive yachts.

Results

All numerical simulations presented in this paper were obtained using Fluent 6. We have used the RANS approach with the segregated solver and the Spalart-Allmaras turbulence model. Preliminary tests (not shown here) have shown that this turbulence model gives better results for this kind of flow than the other tested turbulence models proposed in Fluent 6 (Chapin et al 2003). Hybrid meshes were used with a structured mesh in the inner region adjacent to mast and sail and an unstructured mesh in the outside region. This choice was made to increase flexibility and control in mesh generation, especially for future extension to be able to tackle real complex geometries with multiple sails and masts. Before obtaining reliable results, we performed a grid-sensitivity study and a lot of runs were conducted in order to choose the best numerical parameters. Second-order spatial and temporal schemes were always used. More details about the numerical approach may be found in Chapin et al (2003) and Castanet (2004).

Flow physics around mast-sail geometry

Wilkinson's experimental database, obtained in the 2.13×1.52 m wind tunnel of Southampton University, remains the basis for understanding the differences between experimental measurements and numerical predictions around mast-sail configurations. To our knowledge, it is the only experimental database in open literature that contains mast and sail pressure distributions for a large number of configurations (with various sail cambers and mast diameters). It gives local wall-pressure measurements along the mast and the sail. This local physical information is highly useful for investigating which physical phenomena are captured by the numerical model used (mesh, turbulence model, RANS, or URANS equations).

Wilkinson has shown that in the ranges explored for the parameters ($7.5\% < f/c < 17.5\%$, $4\% < d/c < 17\%$, $3.5 \times 10^5 < \mathrm{Re} < 1.6 \times 10^6$, $2.5 \text{ deg} < i < 10 \text{ deg}$), "all of the apparently different pressure distributions shapes observed during testing were in fact just forms" around the universal pressure distribution presented in Fig. 2. This universal pressure distribution is divided in nine regions representative of a particular physical-flow phenomenon, as described in the table of Fig. 2. A primary question was to see if the RANS simulations around Wilkinson's mast-sail geometry were able to qualitatively capture the same flow features. We have chosen two Wilkinson's mast-sail configurations on which RANS calculations were conducted. In Fig. 3, we present a flow visualization from a RANS calculation around the first case with a mast diameter $d/c = 10\%$ and a camber ratio $f/c = 12.5\%$. Captured recirculation regions on sail suction and pressure sides are clearly seen behind mast separation points. Comparison of Figs. 3 and 4 shows that the shape of the upper-surface bubble is similar to those found in a wind-tunnel test by Wilkinson (1990). A detailed comparison of Figs. 3, 4, and 5 also shows that the reattachment process of the upper-surface bubble is qualitatively well reproduced by the simulation, with a laminar separation over the mast, a high increase of the turbulent viscosity ratio in the following shear layer (Fig. 5), and a turbulent reattachment on the sail, where the experiment found a laminar separation followed

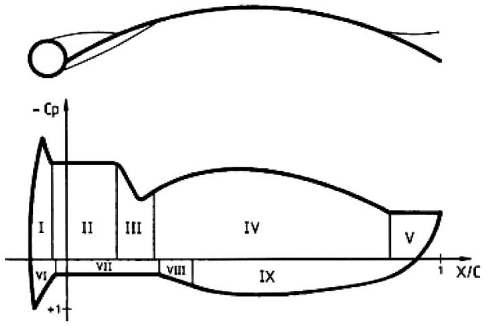

REGION	DESCRIPTION
I	Upper Mast Attached Flow Region
II	Upper Separation Bubble
III	Upper Reattachment Region
IV	Upper Aerofoil Attached Flow Region
V	Trailing Edge Separation Region
VI	Lower Mast Attached Flow Region
VII	Lower Separation Bubble
VIII	Lower Reattachment Region
IX	Lower Aerofoil Attached Flow Region

Fig. 2 Universal pressure distribution (from Wilkinson 1984)

by a bubble transition and a turbulent reattachment (Fig. 4). Figure 6 shows comparisons between RANS calculations and Wilkinson results for the pressure distributions at four aerodynamic angles of attack. The numerical and experimental pressure coefficient distributions are very similar despite the complexity of the flow with mast and sail separations, recirculation regions, and a change in the flow regime inside the upper-surface bubble region. RANS calculations found the same nine regions proposed by Wilkinson (1989) in Fig. 2. Higher differences between experiments and RANS simulations are concentrated in separated-flow regions II and III (upper separation bubble and upper reattachment region) for all aerodynamic angles of attack and in regions V and VII (trailing-edge separation and lower separation bubble) for the lower aerodynamic angle of attack. Attached-flow regions I, IV, VI, and IX (upper and lower mast and sail attached-flow regions) are well predicted. The pressure level of the upper-surface bubble region is well predicted for high incidence angles but, as found by Caponnetto and Castelli (1998), the bubble length is always underestimated (Fig. 6, regions II and III). The trailing-edge separation pressure level is not well predicted for low incidences where separation is small, whereas it is well predicted for higher incidences where separation is larger. This may be related to the high length of the lower bubble at low incidence. Quantitative measurements of the upper-surface-bubble reattachment location and trailing-edge separation point were obtained by Wilkinson (1990) through a finely designed robotic system able to acquire velocity profiles in sail boundary layers. These values and others are reported in Table 1 for comparisons.

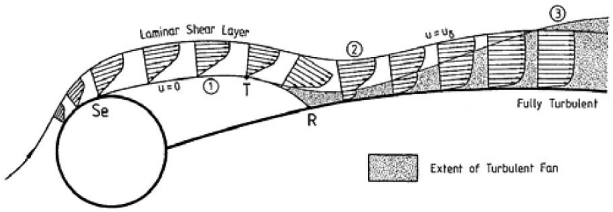

Fig. 4 Upper-surface bubble region from boundary layer analysis (from Wilkinson 1990)

A more detailed study, not shown here, about the location of the bubble reattachment point on the upper surface (Wilkinson's cases number 52/64) has shown that the numerical prediction is sensitive to the spatial scheme order, and was larger with a more resolved mesh along the sail surface and a higher-order scheme. An asymptotic value was obtained through mesh refinement. In this study, we have also found a bubble length dependence to the turbulence model with bubble length underestimation with all tested two equations models, as is well known (Thangam & Speziale 1992). To complete experimental data about separations, we planned wind-tunnel tests on typical wingmast-sail geometries to evaluate separation and reattachment point displacements with variations of sail camber and wingmast angle to correlate in more detail computed and experimental results and increase our understanding of this critical point for rig performance evaluation.

Performance dependence to design parameters

As shown in the previous section, RANS simulations are able to qualitatively capture the main flow features of the mast-sail aerodynamic. In particular, massively separated flow regions and the reattachment process of the upper-surface bubble appear fairly well captured. Differences remain between calculations and experiments, which need to be addressed, but to achieve mast-sail optimization, we just need to predict the right relative performance in response to design parameter variations. As an example, Jones and Korpus (2001) have shown that it was not the case between viscous and inviscid methods for the important design relation between sail camber and aerodynamic finesse or lift-to-drag ratio. One of the motivations of this work was to evaluate the capabilities of RANS methods for this kind of design problem. Hence, we have investigated how a change of a design parameter affects mast-sail performances. RANS simulations were conducted and comparisons with wind-tunnel experiments were done. We illustrate this point with the following four important design parameters: Reynolds number, incidence angle, mast diameter, and sail camber.

Reynolds number effect. Computed results were found to be nearly insensitive to changes in the Reynolds number with

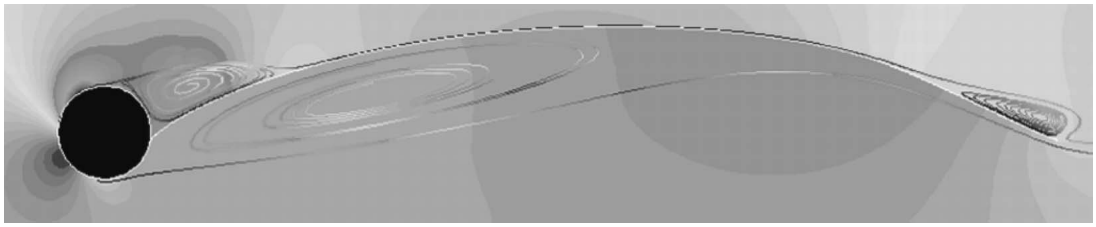

Fig. 3 RANS simulation visualization of a mast-sail configuration (d/c = 10%, f/c = 12.5%, i = 2.5 deg, Re = $1.4 \cdot 10^6$). Background colors = pressure, separations, and bubbles streamlines colored by turbulent viscosity ratio

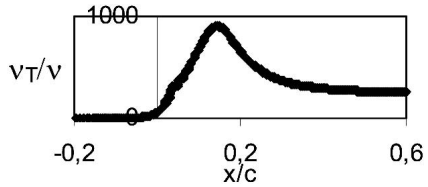

Fig. 5 Turbulent viscosity ratio on the upper-surface separation streamline

a factor two, as was also found experimentally on pressure coefficient distribution in Wilkinson's tests (1989), on aerodynamic coefficients in Milgram (1978), and Haddad and Lepine (2003) water and wind-tunnel tests. Because we do not have detailed experimental results on a larger range of Reynolds numbers, we have not focused on the Reynolds number influence on mast-sail performance in the following sections of the paper.

Incidence angle effect. Experimental and numerical results agree well to capture the incidence angle effect. Figure 6 clearly shows that increasing the incidence angle results in a decrease of the base pressure within the upper-surface bubble (region II) and an increase of the upper-surface bubble length (region III). Increasing incidence also flattened the upper-surface pressure distribution (region IV) and increased the size of the trailing-edge separation (region V), as may be seen in Figs. 6, 7, and 8.

The pressure contribution to lift and drag coefficients versus incidence angle is presented in Fig. 9 (because only wall pressure has been measured in Wilkinson's tests). We may observe a similar behavior of experimental and numerical values with increasing incidence angle. The lift coefficient

Table 1 Separated flow region locations on mast-sail configurations (*f/c* = 12.5%, incidence angle *i* = 5 deg)

Paper Method	Wi 64 Exp.	Present RANS	Wi 52 Exp.	Present RANS
Re	1.0×10^6	1.4×10^6	0.6×10^6	1.4×10^6
d/c	4.3%	4.3%	10.2%	10.2%
θ_{stag}	nr	−44 deg	nr	−27 deg
θ_{se1}	nr	64 deg	nr	85 deg
x_{re1}	0.13	0.09	0.31	0.16
x_{se2}	0.80	0.85	0.82	0.83
θ_{si1}	nr	−109 deg	nr	−107 deg
x_{ri1}	nr	0.35	nr	0.68

Wi 52, Wi 64 = Wilkinson's case numbers 52, 64

obtained numerically was slightly higher than the experimental one except for the smallest incidence angle, $i = 2.5$ deg, which was the more difficult to predict, as seen in the previous part. Numerical pressure drag behavior with incidence angle was also coherent with experimental values. As expected, differences were higher than for the lift coefficient but fairly reasonable, knowing that to be representative, these differences should be compared to the total mast-sail drag (pressure + friction + induced drag components). We may conclude that main flow feature behavior was in agreement between experiments and RANS prediction.

Quantitative differences found may be mainly attributed to the fact that RANS simulations underestimate upper-surface bubble length at all incidence angles and base pressure level at low incidences (cf. Figs. 6, 7, and 8). This fact results in an underestimation of the lift coefficient.

Quantitative differences may also be partly related to the

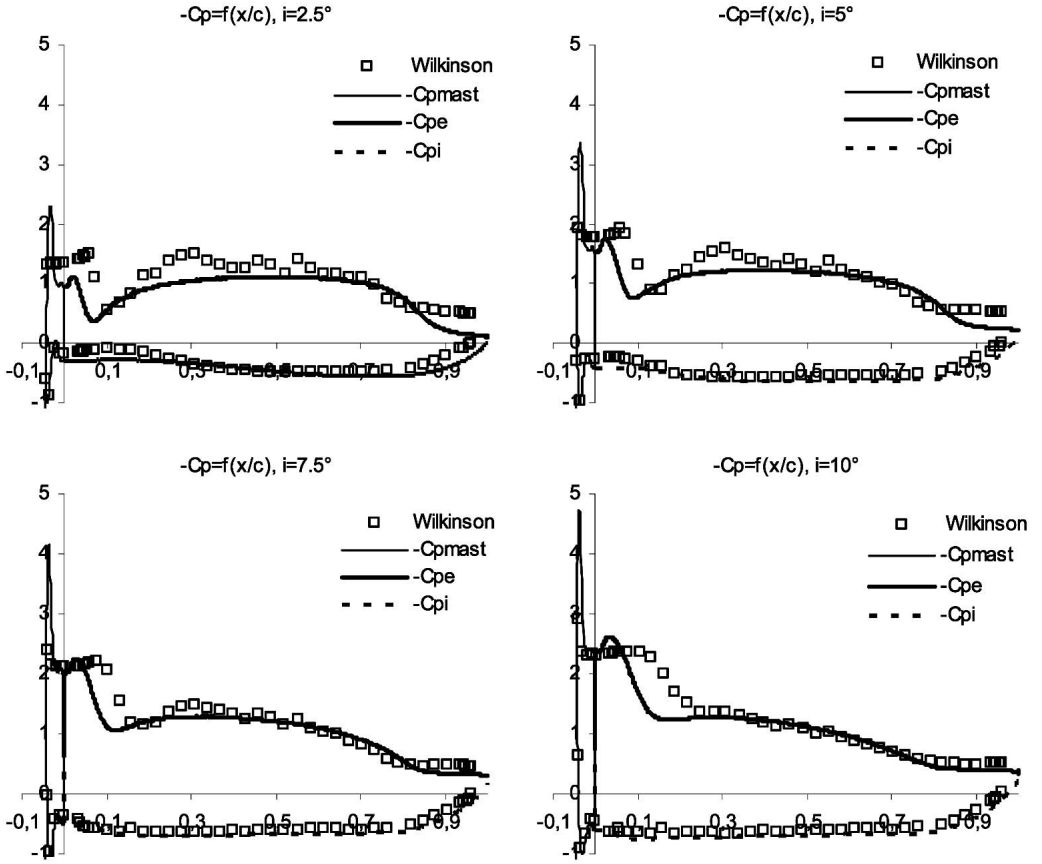

Fig. 6 Pressure coefficient distribution $-C_p = f(x/c)$ at four wind incidence angles (comparison between present RANS simulations and experimental data from Wilkinson 1984)

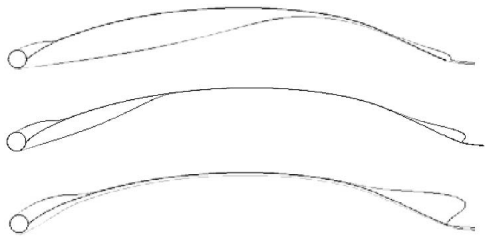

Fig. 7 Separation streamlines versus wind incidence angle. (Top) i = 2.5 deg. (Middle) i = 5 deg. (Bottom) i = 10 deg

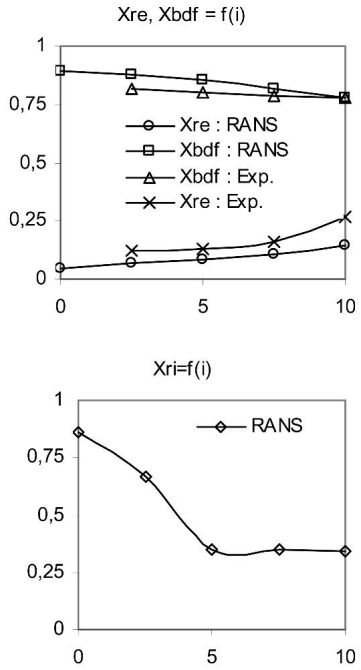

Fig. 8 (Top) Upper-surface bubble reattachment point and trailing edge separation point versus incidence angle. (Bottom) Lower-surface bubble reattachment point versus incidence angle

not-documented three-dimensional character of Wilkinson's tests compared to the perfectly two-dimensional character of the numerical simulations. The sail aspect ratio was only 3, and wind-tunnel walls were used as endplates with a nonzero gap. Tests on classical wings done by Mueller (1999) clearly show that three-dimensional effects associated with the presence of endplates may lead to an underestimation of the lift coefficient when measured with a force balance. However, more detailed wind-tunnel tests, with documented three-dimensional effects or high aspect-ratio sails, would be necessary to further increase the analysis. In this context, a relevant test program is planned in the large wind-tunnel test section S4 at Ensica fluid mechanics department.

To conclude, the present comparison between numerical and experimental results appears as fairly reasonable for these complex, massively separated flows and shows that the well-used RANS method may be considered as a relevant tool to investigate mast-sail relative performances with a design objective.

Mast diameter *d/c* effect. In our RANS simulations, as in Wilkinson's experiments, we found a similar pattern of pressure distributions with mast diameter variations. As an example, we may see on Fig. 10 that when d/c was increased, the length of the upper-surface bubble was increased, the length of the lower-surface bubble was highly increased, the

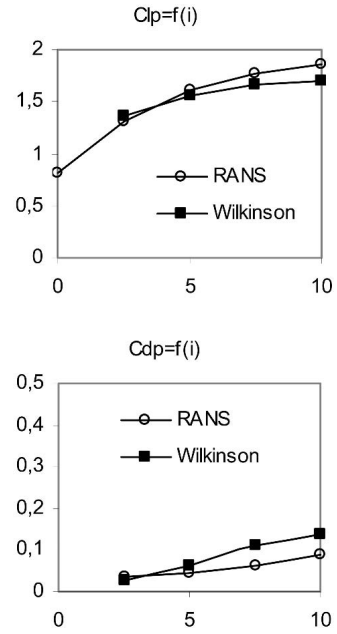

Fig. 9 Experimental/numerical comparison of pressure lift and drag versus incidence angle. Experimental case: Wilkinson 1984, d/c = 4.3%, f/c = 12.5%, Re = 1.4e6. Numerical case: same conditions with RANS approach and Spalart-Allmaras turbulence model

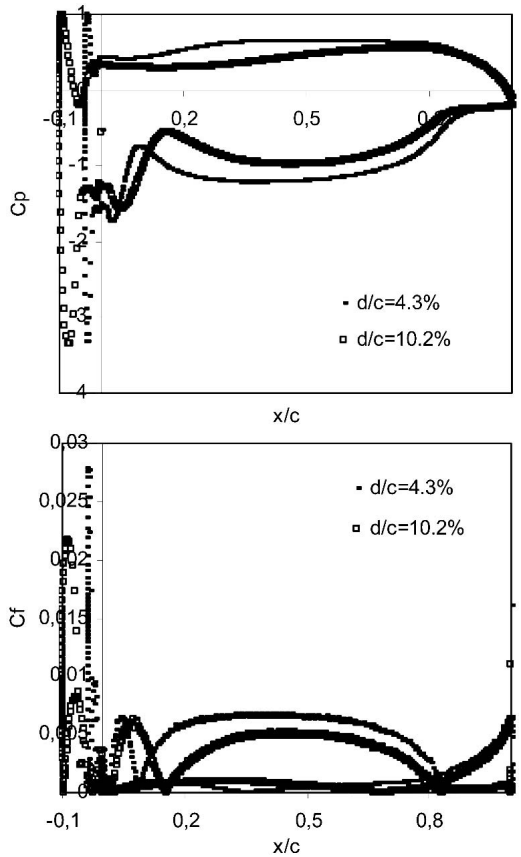

Fig. 10 RANS prediction of the mast diameter effect on pressure and wall friction coefficients distribution with i = 5 deg, Re = 1.4 · 10^6

severity of the pressure recovery at reattachment and the suction dome was reduced. We also see that when d/c increases, the base pressure increases on the lower surface and decreases on the upper surface, which results in a lift coeffi-

cient decrease. Despite this, the size of the upper-surface trailing-edge separation (Fig. 10, Table 1) was found to be nearly independent of mast diameter in the range tested, as was found in Wilkinson's measurements.

Sail camber ratio *f/c* effect. Wilkinson found that the camber ratio *f/c* had little effect on the upper-surface bubble base pressure, which decreased a little with increasing camber ratio. He also found a small decrease of the upper-surface bubble length with increasing camber ratio. Figure 11, numerical results obtained on a larger range of camber ratio (3% to 16% vs. 7.5% to 12.5%), shows the same tendencies with a higher-amplitude variation of the base pressure in the upper-surface bubble except for the lowest camber ratio *f/c* = 3% where the absence of suction dome on the sail results in a large upper-surface bubble with a low base pressure and then in a poor mast-sail performance. For camber ratio variations in the range investigated by Wilkinson, experiments and numerical results behavior were in good qualitative agreement, as summarized in Table 2. They show that the reattachment pressure recovery (region III) became more intense and the suction dome (region IV) much fuller with increasing camber ratio. They also show that the trailing-edge separation (region V) grew with increasing camber ratio, while its base pressure was reduced (cf. Fig. 11).

Application to mast-sail design

Having assessed that RANS simulations and experiments give the same tendencies under changes of relevant design parameters (Re, *i*, *d/c*, *f/c*), we may try to do RANS-based optimization of the mast-sail design to show its high interest in real separated viscous flows around mast-sail geometries. To illustrate the relevance of this approach, we have chosen two examples.

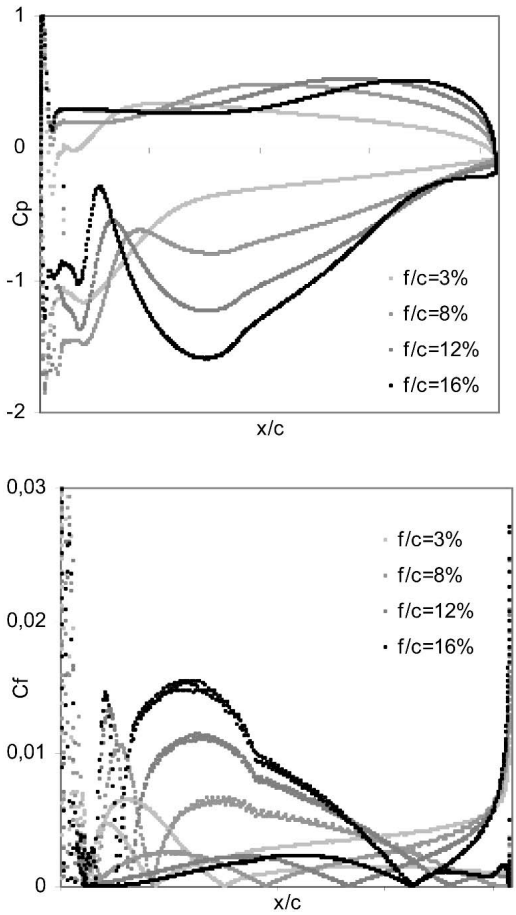

Fig. 11 RANS prediction of the sail camber ratio effect on pressure and wall friction coefficients distribution with d/c = 5%, $i = i_{opt}$ = 4 deg

Table 2 Sign of the variables derivatives versus parameters (*i, d/c, f/c*) as found by RANS simulations and wind-tunnel experiments

Paper Approach	Wi 84 Exp.	Present RANS
$\partial L_{\text{upper bubble}}/\partial i$	+	+
$\partial L_{\text{upper bubble}}/\partial(d/c)$	+	+
$\partial L_{\text{upper bubble}}/\partial(f/c)$	−	−
$\partial Cp_{\text{upper bubble}}/\partial i$	+	+
$\partial Cp_{\text{upper bubble}}/\partial(d/c)$	−	−
$\partial Cp_{\text{upper bubble}}/\partial(f/c)$	−	−
$\partial L_{\text{sep bdf}}/\partial i$	+	+
$\partial L_{\text{sep bdf}}/\partial(d/c)$	0	0
$\partial L_{\text{sep bdf}}/\partial(f/c)$	+	+
$\partial L_{\text{lower bubble}}/\partial i$	−	−
$\partial L_{\text{lower bubble}}/\partial(d/c)$	++	++
$\partial L_{\text{lower bubble}}/\partial(f/c)$	++	++

Wi 84 = Wilkinson 1984

The first one is intended to show that RANS methods are able to find an optimum camber ratio $(f/c)_{opt}$ for a given mast-sail configuration. The existence of such an optimum camber in a given environment is well known by competitive sailors, as reported by Bethwaite (1996) from championships results and found in preliminary low-Reynolds-number wind-tunnel experiments (Haddad & Lepine 2003) but is not yet included in classic VPP aerodynamic models.

The second example aims at investigating what can be learned about the mast-sail strong interaction and its main consequence, the fact that the mast-sail drag is not equal to the sum of mast and sail drag components as measured or computed separately around each structure in a free stream.

Optimum sail camber ratio. An important question for the sail designers is to know the sail optimum camber for a given rig, boat, and sailing condition. For a rigorous quantitative assessment of a sail performance, it will be necessary to use a full yacht performance evaluation through a VPP calculation with known hull hydrodynamic data. This is not really possible at this sail design stage, and we need a simplified approach to evaluate rig design in general terms without reference to a particular hull. Here, optimum will be considered in the sense that it maximizes the sail finesse (lift-to-drag ratio), for a given lift coefficient. Hence, high lift values will be representative of light wind conditions (without limitation on the heeling moment) and lower lift values will be representative of medium to strong wind conditions (with a limitation on the heeling moment).

The existence of this optimum sail camber ratio is a direct consequence of the nonlinear behavior of the aerodynamic coefficients with camber variation as a result of viscous flow separation. This fact was one major motivation to use RANS methods because widely used vortex lattice methods cannot handle viscous flow phenomena and by consequence cannot predict this kind of optimum sail camber ratio.

Before going to RANS results, we briefly show through aerohydrodynamic force equilibrium equations why it is important to maximize sail finesse for a given lift coefficient. If we look at the aerohydrodynamic forces equilibrium with a no-heel hypothesis (Fig. 12), we can write the following relations (Marchaj 1962):

$$F_{lh} = F_{ha}$$
$$F_{dh} = F_{ra}$$

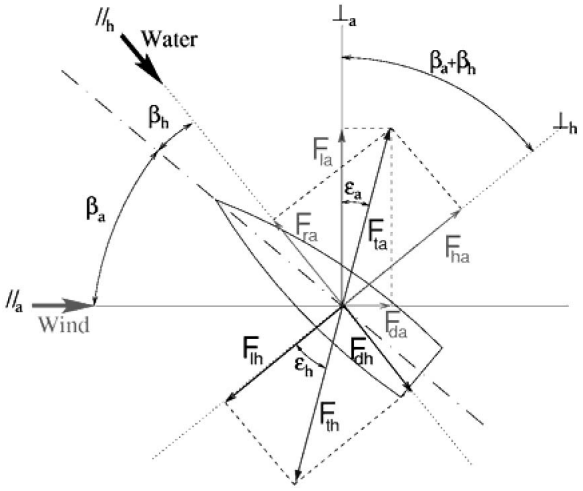

Fig. 12 Aerohydrodynamic forces equilibrium in the horizontal plane

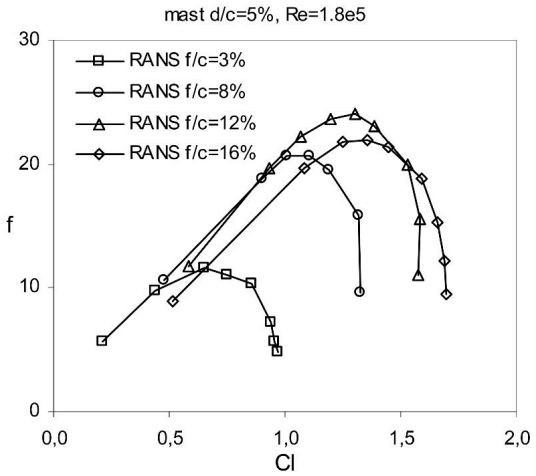

Fig. 13 Camber ratio *f/c* effect on mast-sail performance

which is equivalent to

$$\beta_a + \beta_h = \varepsilon_a + \varepsilon_h \equiv \text{Arctg}(1/f_a) + \text{Arctg}(1/f_h) \qquad (1)$$
$$F_{ta} = F_{th}$$

with f_a the aerodynamic finesse and f_h the hydrodynamic finesse defined by:

$$f_h \equiv F_{lh}/F_{dh}$$
$$f_a \equiv F_{la}/F_{da} \equiv C_l/C_d$$

and β_a the apparent wind angle, β_h the leeway angle. Then, with the aerohydrodynamic equilibrium we can write

$$f_h \equiv F_{lh}/F_{dh} = F_{ha}/F_{ra} \equiv C_h/C_r$$

and relations between the aerodynamic coefficients (C_l,C_d) and the propulsive and the heeling force coefficients (C_r, C_h) can be written:

$$C_r = C_l \sin(\beta_a + \beta_h) - C_d \cos(\beta_a + \beta_h)$$
$$C_h = C_l \cos(\beta_a + \beta_h) + C_d \sin(\beta_a + \beta_h)$$

When the speed of a displacement sailing yacht increases, the hydrodynamic drag F_{dh} increases more rapidly than the hydrodynamic lift F_{lh}, which increases with the yacht speed square. Hence, the hydrodynamic finesse $fh = F_{lh}/F_{dh}$ decreases with the yacht speed increase. Also, because the equilibrium equation (1) is verified, for a given water/wind angle $\beta_a + \beta_h$, the yacht speed increases only if the aerodynamic finesse increases. Also, for a given sailing yacht, the higher the aerodynamic finesse f_a, the higher may be the yacht speed. From this simple equilibrium consideration, it is clear that for a given value of the water/wind angle, $\beta_a + \beta_h$, there is a relation between the maximum aerodynamic finesse and the maximum yacht speed.

With this in mind, we may look at RANS results for mast-sail configurations with $d/c = 5\%$ and sail camber ratio $f/c = 3\%$, 8%, 12%, and 16%, as presented in Fig. 13. The plot of aerodynamic finesse versus lift coefficient clearly shows that the RANS approach captures an optimum camber value of about 12% where the aerodynamic finesse reaches its maximum. To our knowledge, it is the first published numerical estimation of an optimum sail camber. Moreover, the optimum camber value found compares favorably to Bethwaite's analysis, which shows that the optimum sail camber is around 13% for classical cylindrical masts, as considered here, and around 10% for oriented wingmast. This RANS-based camber optimization of mast-sail configurations seems promising and illustrates the potential of these advanced numerical methods to design, analyze, and increase our understanding of the complex separated flows that take place around complete sailing yacht rigs. Moreover, it will be easy to generalize this approach to more complex geometries through the hybrid nonconformal mesh technology used here.

Mast-sail design. The second example chosen to illustrate the potential of RANS-based analysis in mast-sail design considers the mast-sail interaction and its impact on mast-sail performances. Usually, sail design and mast design are done separately and the additive hypothesis is used to say that, from the aerodynamic point of view, the lower the mast drag and the lower the sail drag, the better the design of the mast-sail will be. However, Milgram's wind-tunnel experiments in 1978 showed that drag due to the addition of a mast to a sail results in a complex flow interaction and must not be taken as the sum of the mast drag and the sail drag as measured or computed separately in a free stream. Our objective is to show the agreement of RANS-based numerical simulations with experiments about the strong mast influence on sail performance and the ability of this numerical approach to capture a mast-sail drag that takes into account the strong interaction between the mast and the sail. This problem is of high importance because, as an example, sailing people are not in agreement regarding whether it is better to have a thin mast with more spreaders or to have a thicker mast with fewer spreaders. In fact, this is a complex multidisciplinary problem that may be partly clarified by a good use of RANS-based simulations. This complex design choice was illustrated in the last two America's Cups by Team New Zealand rigging choices with a three-spreader mast in 2000 and a four-spreader mast with a thinner section in 2003. What is the best choice?

Remarks about the mast effect. As is well known and may be seen on RANS results in Fig. 14, the optimum value for mast diameter (d/c) is zero. The higher the d/c, the lower the lift and the higher the drag. The main effect of the mast in the leading-edge region of the sail was clearly on the lift-to-drag ratio, mainly in the high lift region of the curve, which is the region of interest. The maximum lift coefficient is nearly not affected. The lift-to-drag ratio increases nearly 200% when we add a mast of only 5% of the sail chord ($d/c = 5\%$). This impact will not be as high on a real three-dimensional mast-sail configuration because of the induced drag component, but we need to have in mind Marchaj's experiment, which emphasized the mast effect on a real three-dimensional rig through a wind-tunnel experiment (Marchaj 1976). He showed in his paper that numerical pre-

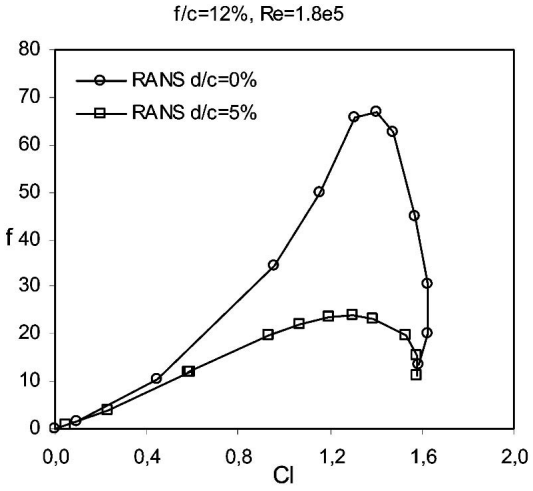

Fig. 14 Mast diameter effect on sail performance for camber ratio *f/c* = 12%

diction based on inviscid methods overestimates the benefit of high aspect ratio sail in comparison to the detrimental effect of the nondimensional mast diameter *d/c*. His wind-tunnel experiment showed that an increase of the sail aspect ratio without change of the mast height may give a lower performance without change of the mast diameter *d*, because the nondimensional mast diameter *d/c* increases with the decrease of the sail chord *c*.

Hence, the mast primarily affects the minimum apparent wind angle accessible, which increases drastically when the lift-to-drag ratio decreases (see equation 1). Secondarily, the mast affects the boat speed in upwind sailing conditions with medium to strong wind conditions when the lift coefficient used is lower and the aerodynamic finesse reaches highest values.

Mast-sail interaction. In Fig. 15, we presented the RANS results of drag coefficient versus lift coefficient for a sail alone and one mast-sail configuration. We have added the mast-alone drag as evaluated in classical VPP to the sail-alone drag curve to take into account the mast effect. This figure clearly shows that the interaction is significant. We see that the mast-sail configuration has less drag for low values of the lift coefficients and more drag for high values of the lift coefficients. It is shown that the mast effect is not simply additive but is highly dependent on the considered lift

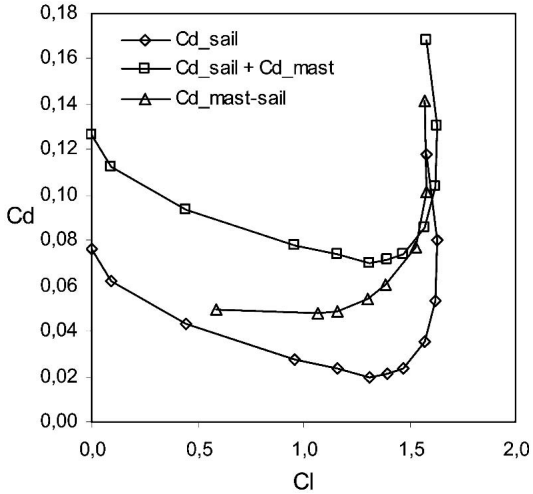

Fig. 15 Mast-sail strong interaction and the related drag nonadditivity

coefficient. Milgram's experiments showed the same result (Milgram 1978).

Two conclusions may be drawn. The first one is that the interaction drag is not a constant but a function of the lift coefficient considered. The second one is that RANS-based numerical simulations, which take into account viscous effects, may be used to evaluate the interaction drag as a function of the lift coefficient. This may be useful to define a better mast aerodynamic model able to take into account the nonlinear drag and lift effects for advanced VPP.

Conclusions

This paper has shown how the use of RANS equations to do numerical simulations around mast-sail geometries with the hybrid nonconformal meshing technology may be of high value in mast-sail design and analysis. Well used, these advanced numerical methods are able to take into account viscous-flow phenomenon induced by strong adverse pressure gradients, such as separation, recirculation bubble, and their nonlinear effects on performances and design choices, such as sail camber and mast diameter. A particularly interesting property found was the ability of the Spalart-Allmaras turbulence model to mimic the transition process on the upper-surface bubble shear layer after mast separation and before turbulent reattachment on the sail.

The existence of an optimum camber for sails is well known by sailors, while ignored by VPPs. It has been shown, probably for the first time, that advanced numerical simulations, based on RANS equations, were able to find sail optimum camber of a mast-sail geometry. Moreover, the optimum camber value predicted compares favorably with Bethwaite's analysis.

The mast-sail strong interaction has been well represented by RANS methods. Our RANS results about the nonadditivity of mast-sail drag has been found in agreement with experimental results and may be used to define a better aerodynamic mast model for advanced VPPs.

Nevertheless, to go further, well-controlled and reliable wind-tunnel databases on detailed flow features around simplified three-dimensional mast-sail geometries are needed to enhance our understanding of these complex separated flows and validate advanced numerical simulations on three-dimensional sailing yacht rigs. This is a preliminary step to tackling the challenging problem of better discriminating the part of three-dimensionality, unsteadiness, turbulence model, and RANS hypothesis in the remaining discrepancies between numerical and experimental results. Then it should be possible to enhance the prediction of bubble recirculation regions, trailing-edge separation, and their spanwise structure. In that direction, three-dimensional unsteady Reynolds averaged Navier-Stokes (URANS) should be evaluated, because this approach seems to be an efficient tool in complex three-dimensional unsteady separated flows, such as a surface-mounted cube, to improve the predictions of the pressure level and length of recirculation regions (Iaccarino & Durbin 2000).

Acknowledgments

The authors wish to acknowledge the people who participated in this work: R. Neyhousser from Y. Parlier Aquitaine Design Team, F. Haddad for discussions, and students B. Haddad, B. Lepine, and S. Castanet for their contributions. Thanks are also expressed to J. B. Cazalbou for his help; H. Belloc, G. Busnel and W. Richard for their support on the experimental part; and Ensica for the support of this activity. This research was partly funded by the Y. Parlier–Hydraplaneur project. Dr. S. Wilkinson is gratefully ac-

knowledged for his permission to use two figures from his work (Figs. 2 and 4).

References

BETHWAITE, F. 1996 *High performance sailing,* Waterline Books, Shrewbery, England, 209.

CAPONNETTO, M., AND CASTELLI, A. 1998 America's Cup yacht design using advanced numerical flow simulations, *EPFL Super Computing Review*, **10,** 97–104.

CASTANET, S. 2004 *Simulation numérique de l'écoulement 2D décollé autour d'un mât et d'une voile*, Rapport de stage de fin d'étude, ENSIAME.

CHAPIN, V. G., JAMME, S., HADDAD, B., AND LEPINE, B. 2003 Ecoulements 2D décollés autour d'un mât et d'une voile, VIIème Rencontre Fluent France, Octobre 15–16, Paris.

COWLES, G., PAROLINI, N., AND SAWLEY, M. L. 2003 Numerical simulation using RANS-based tools for America's Cup design, *Proceedings*, 16th Chesapeake Sailing Yacht Symposium, March, Annapolis, MD.

DURBIN, P. 1995 Separated flow computations with the κ-ϵ-ν^2 model, *AIAA Journal*, **33**, 4.

FLUENT. 2003 *FLUENT 6.1 User's Manual*, Fluent, Inc.

HADDAD, B., AND LEPINE, B. 2003 *Etude expérimentale de l'interaction mât-voile*, Rapport de stage de fin d'étude, Ecole Navale.

IACCARINO AND DURBIN. 2000 Unsteady 3D RANS simulations using v^2-f model, *CTR Annual Research Briefs*.

JONES, P., AND KORPUS, R. 2001 International America's Cup class yacht design using viscous flow CFD, *Proceedings*, 15th Chesapeake Sailing Yacht Symposium, January, Annapolis, MD.

MARCHAJ, C. A. 1962 *Sailing Theory and Practice*, McGraw-Hill, New York.

MARCHAJ, C. A. 1976 *A Critical Review of Methods of Establishing Sail Coefficients and Their Practical Implications in Sailing and in Performance Prediction*.

MILGRAM, J. H. 1971 *Section Data for Thin Highly Cambered Airfoils in Incompressible Flows*, NASA CR-1767, July.

MILGRAM, J. H. 1971 Sail force coefficients for systematic rig variations, *Transactions of the Society of Naval Architects and Marine Engineers,* 10.

MILGRAM, J. H. 1978 Effects of masts on the aerodynamics of sail sections, MARINE TECHNOLOGY, **15**, 1, 35–42.

MILGRAM, J. H., PETERS, D. B., AND ECKHOUSE, D. N. 1993 Modelling IACC sail forces combining measurements with CFD, *Proceedings*, 11th Chesapeake Sailing Yacht Symposium, Society of Naval Architects and Marine Engineers, 65–73.

MILGRAM, J. H. 1998 Fluid mechanics for sailing vessels, *Annual Review of Fluid Mechanics*, **30**, 613–653.

MUELLER, T. J. 1999 Aerodynamic measurements at low Reynolds numbers for fixed wings micro-air vehicles, RTO AVT/VKI special course, September 13–17.

VAN OOSSANEN, P. 1993 Predicting the speed of sailing yachts, *Transactions of the Society of Naval Architects and Marine Engineers*, **101**, 337–397.

SAWLEY, M. L. 2002 Numerical flow simulation for America's Cup: a challenge for researchers and students, *EPFL Supercomputing Review,* May, 13, 4–8.

THANGAM, S., AND SPEZIALE, C.G. 1992 Turbulent flow past a backward-facing step—a critical evaluation of two-equation models, *AIAA Journal,* **30**, 5, 1314–1320.

WILKINSON, S. 1984 *Partially Separated Flows Around 2D Masts and Sails*, Ph.D. thesis, University of Southampton, UK.

WILKINSON, S. 1989 Static pressure distributions over 2D mast/sail geometries, MARINE TECHNOLOGY, **26**, 4, 333–337.

WILKINSON, S. 1990 Boundary layer explorations over a 2D mast/sail geometry, MARINE TECHNOLOGY, **27**, 250–256.

WYNNE, J. 2002 Simulation numérique de l'ecoulement de l'air autour du class America Alinghi, EPFL semester project.